Regular Article

ANALYTICAL
AND BIOANALYTICAL
CHEMISTRY
RESEARCH

Published by the
Iranian Chemical Society

***Anal. Bioanal. Chem. Res.**, Vol. 10, No. 3, 251-268, July 2023.*

Removal of Cr(III), Pb(II) and Cr-Pb Mixture by Blast Furnace Slag (BFS) in Solution

Toufik Chouchane*, Ouahida Khireddine, Sana Chibani and Ateman Boukari

Research Center in Industrial Technologies CRTI, P. O. Box: 64, Cheraga 16014 Algiers Algeria

(Received 10 October 2022, Accepted 23 November 2022)

Blast furnace slag (BFS) was exploited as an adsorbent for the removal of Cr(III), Pb(II), and Cr-Pb. In discontinuous mode, the influence of the contact time, stirring speed, pH, mass of the adsorbent, initial concentration, and temperature were examined. The physico-chemical tests indicated that the BFS is formed from a mixture composed mainly of silicates, aluminates, lime, and magnesium oxide. Its specific surface is 325.6 $m^2 g^{-1}$ and the pH_{zpc} value corresponds to 3.8. Experimental results have indicated that the equilibrium is obtained after 60, 50, and 80 min for Cr(III), Pb(II), and the Cr-Pb mixture, respectively. Under our experimental conditions (pH 4.8, V_{ag}: 150 rpm, T: 20 °C, Øs: 200 µm, and Ms: 1 g), the adsorption capacities of Cr(III), Pb(II), Cr-Pb, Cr(III) in the mix, and Pb(II) in the mix were 43.16, 50.12, 39.91, 17.05, and 22.66 mg g^{-1}, respectively. Moreover, BFS has more affinity for lead in the binary mixture. The adsorption isotherms revealed that the Langmuir model was the best fit for the metal ion adsorption processes examined ($R^2 = 0.99$). The kinetics indicated that the adsorption of the metal ions studied follows the pseudo-second-order model and that their transfers from the solution to the adsorbent are controlled by external and intraparticle diffusion. The thermodynamic study has shown that all the processes applied are spontaneous, exothermic, and less entropic. The desorption of the binary mixture revealed that saturated BFS can be efficiently exploited over four cycles, and it is more efficient in the presence of HCL at 0.1 N.

Keywords: Blast furnace slag, Cr(III), Pb(II), Kinetics, Adsorption isotherm

INTRODUCTION

Urban and industrial development have generated considerable ecological damage caused by harmful inputs such as heavy metals (Hg, Cr, Cd, Pb, Ni, and others) [1,2]. The latter has the power to accumulate in the digestive tract of humans, which is harmful to their health [3]. In the sea, they destroy sea nests. On the other hand, in irrigation water, they cause damage all along the food chain [4]. The removal of these toxic elements from liquid influents is of capital interest for most industrialized countries because they generate serious problems for humans and their environment [5,6].

In this context, important processes have been adopted for the protection of the environment. namely chemical precipitation [7], membrane techniques [8], ion exchange [9], coagulation-flocculation [10], and adsorption [11]. Among these technologies, adsorption has been selected as a treatment of choice because of its effectiveness. In addition, it is simple and easy to execute, regenerates less mud, and consumes less energy [12]. According to the literature, several adsorbents have been used in this process, such as activated carbon [13], graphene oxide [14], bentonite [15], kaolin [16], sawdust [17], biochar [18], metal-organic framework [19] and green adsorbents [20].

In this perspective, we focused on the elimination of Pb(II), Cr(III), and the Cr-Pb binary mixture in solution on the BFS by the adsorption process. The main objectives of this work were to optimize the determining parameters, measure the adsorption capacities, and study the kinetics,

*Corresponding author. E-mail: chouchane_toufik@yahoo.fr

mechanism, and nature of adsorption of the ions examined on the BFS.

Blast furnace slag is formed during the production of liquid cast iron in the steel industry. It consists mainly of CaO, SiO_2, Al_2O_3, and an insignificant amount of metals [21]. In the past, blast furnace slag has been used as hydraulic cement, concrete aggregate, and pavement materials. Currently, and with technological evolution, it has been oriented toward the field of water pollution control [22].

According to Chouchane *et al*. [21], it was demonstrated that the slag from the blast furnace of the El Hadjar complex has the capacity to adsorb 53.58 mg of nickel per gram in solution after 90 min of stirring. Ngoc Lee *et al.* [23] have reported that the blast furnace slag converted to slag oxalate showed a fast adsorption rate and a very high maximum cobalt adsorption capacity (576 mg g^{-1}). C. Li *et al*. [24], specified that the blast furnace slag transformed into hydroxyapatite-zeolite presented a high adsorption performance for the elimination of Mn^{2+}, NH^{4+}, and phosphate ions diluted in water. Kim *et al.* [25] showed that arsenic elimination by adsorption on basic oxygen furnace slag is feasible at pH between 7 and 11. On the other hand, at pH 12, its elimination is caused by chemical precipitation. The work carried out by L. Wang *et al.* indicated that steelworks slag as an adsorbent presents a good opportunity for the removal of copper and lead in the flotation wastewater [26]. Y. Xue *et al.* [27] showed that basic oxygen furnace slag as an adsorbent possesses the power to adsorb a mixture of metal ions consisting of Cu, Cd, Pb, and Zn at different percentages.

Treated heavy metals, namely chromium and lead, are generally detected in industrial liquid discharges. They are harmful to humans, vegetation, and aquatic life even at low levels [2,28]. From the literature, it has been mentioned that the removal of these toxic elements has been the subject of various research works, where several processes have been used [29-31].

In this research, certain determining parameters such as the contact time, pH of the medium, the temperature of the solution, initial concentration of the adsorbate, and mass of the adsorbent were exploited to explicate the kinetics, mechanisms of interaction, and the nature of the adsorption process. X-ray fluorescence, Fourier transform infrared (FTIR), and X-ray diffraction analyzes were used for the characterization of the solid. The specific surface was evaluated by the model of Brunauer, Emmett, and Teller.

METHODS/EXPERIMENT

Blast Furnace Slag Treatment

The solid slag samples taken at the level of the blast furnace of the Sider El Hadjar complex were prepared and treated according to the protocol presented by Chouchane *et al.* [21].

Analytic Methods

The residual concentrations of metal ions were determined by atomic absorption spectrometry (Perkin Elmer 3110, France). The pH of the solution was measured using a pH meter (Ericsson). Characterization of the solid was carried out by X-ray fluorescence (Siemens SRS 3000), X-ray diffraction (Rigaku Ultim IV, Germany) and Fourier transform infrared spectrometer (Perkin Elmer, France). The specific surfaces were measured using the model of Brunauer, Emmett, and Teller (BET model, Germany). The agitation of the solution is provided by a mechanical rod stirrer (SE 100). The temperature of the medium is controlled by a laboratory pyrometer.

Specific Surface Area Determination

The specific surface area of the treated blast furnace slag sample was determined from the amount of nitrogen adsorbed as a function of its pressure. This process was carried out at the boiling temperature of liquid nitrogen (-196 °C) and under normal atmospheric pressure (760 mm Hg) [21]. The experimental data of N_2 gas desorption at 77K were evaluated with the BET model [32].

Process of Adsorption of Metal Ions Alone and in Mixture

Adsorption experiments in the batch mode were carried out in order to valorize the slag as an adsorbent for the removal of Pb(II), Cr(III), and Cr-Pb mixture in solution. The experimental approach requires introducing 01 g of slag into a solution containing the pollutant or pollutants to be eliminated in a beaker of 01 l in volume. Pb(II) was obtained by dissolving lead nitrate in bidistilled water ($Pb(NO_3)_2$, $6H_2O$). Cr(III) was created by dissolving trivalent chromium

nitrate ($Cr(NO_3)_3$, $9H_2O$) in bidistilled water. Solutions of the Cr-Pb binary mixture consisting of 50% Cr(III) and 50% Pb(II).

The experimental approach was carried out according to the mode presented by Chouchane *et al.* [21].

The capacity absorbed at equilibrium (q_e), the capacity adsorbed at time t (q_t), the elimination rate and the distribution coefficient (k_d) are presented by Eqs. (1)-(4).

$$q_e = \frac{C_0 - C_e}{m} \times V \quad (1)$$

$$q_t = \frac{C_0 - C_t}{m} \times V \quad (2)$$

$$\%R = \frac{C_0 - C_e}{C_0} \times 100 \quad (3)$$

$$k_d = \frac{C_i - C_e}{C_e} \times \frac{V}{M} = \frac{q_e}{C_e} \quad (4)$$

Where qe: capacity absorbed at equilibrium (mg g^{-1}), q_t capacity adsorbed at time t (mg g^{-1}), C_0: initial concentration (mg l^{-1}); C_e: concentration at equilibrium (mg l^{-1}), k_d: distribution coefficient (l g^{-1}), m: adsorbent mass and V; solution volume

Point of Zero Charge

The point of zero charge is the pH value of the solution when the charge of the superficial surface is zero. The pH < pHzpc indicates that the surface is positive, which favors the adsorption of anionic ions. Otherwise (pH > pHzpc), indicates that the surface is negative, which favors the adsorption of cationic ions. The point of zero charge is determined by the procedure presented by T. Chouchane *et al.* [33]. In this step, potassium chloride solutions at 0.1 and 0.01 N were used in order to specify the impact of the ionic strength of the solutions and to define the ZPC. The mass of the adsorbent used is 2 g.

Desorption Process

The amount of saturated BFS that was utilized in this desorption process is 10 g. The saturated BFS samples recovered after filtration were baked at 105 °C for 24 h. The desorption process was performed using distilled water and different eluents, namely sulfuric acid (0.1 N), nitric acid (0.1 N), and hydrochloric acid (0.1 N).

RESULTS AND DISCUSSION

Characterization of BFS

The BFS from the Sider El-Hadjar complex is mainly composed of alkaline oxides (CaO and MgO) and acidic oxides (Al_2O_3 and SiO_2). where the rate of CaO is 37.2%, MgO is 3.12%, Al_2O_3 is 8.2%, and SiO_2 is 41.1% (Table 1). In addition, BFS has a small amount of other metal oxides (Fe_2O_3, NiO, K_2O, and Na_2O) (Table 1).

Table 1. Chemical Composition of BFS [21]

Element	%Massique
CaO	37.2
Al_2O_3	8.2
SiO_2	41.1
Fe_2O_3	2.51
MgO	3.12
MnO	2.64
K_2O	0.3
Na_2O	0.7
P.A.F	4.23

The tests realized by X-ray diffraction indicated that the BFS is essentially composed of lime, silica, and alumina in less quantity (Fig. 1a). The FT-IR spectrum of this fraction shows the stretching vibrations of 1793, 879, and 715 cm^{-1} whose origins are due to the stretching vibration of $COCa_3$ (Fig. 1a). The CO bond elongation was indicated by the observed peak at 1437 cm^{-1}. However, the Si-O-Si and Al-O bonds were indicated by the vibration bands, respectively: 1007 cm^{-1}, and 634 cm^{-1} (Fig. 1b). These observations were justified by the results obtained by the analyses performed by X-ray fluorescence.

The specific surface areas of the BFS particles were obtained by using the nitrogen gas adsorption-desorption method. The isotherm data for nitrogen gas desorption at 77 k were analyzed with the Brunauer, Emmett, and Teller model (model BET). The investigations revealed that the specific surface is 325.6 m^2 g^{-1}. In this work, the pHzpc of modified blast furnace slag was evaluated. Experimental data showed that the pH of the zero point of charge is around

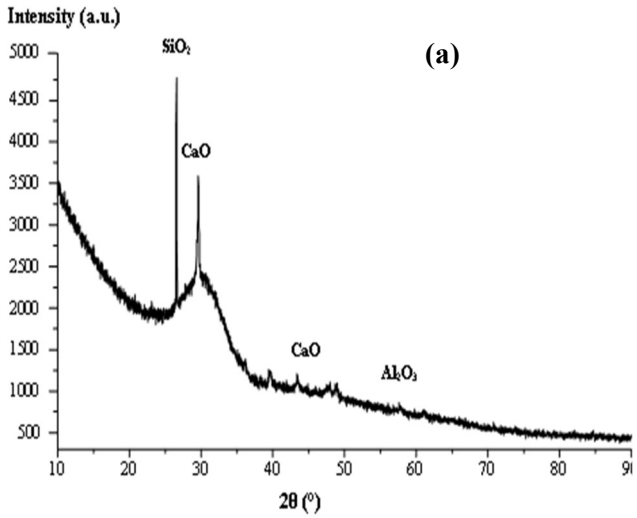

Fig. 1. (a) Diffractogram of BFS sample [21], (b) infrared spectrum of BFS sample.

3.8 (Fig. 3c).

Effect of Agitation Speed

The agitation of the solution (V_{ag}) is an essential step in these processes since it contributes to the diffusion of the adsorbate towards the adsorbent [29]. The agitation speeds used corresponded to 50, 100, 150, and 200 rpm. The experimental conditions applied are: C_O = 30 mg l^{-1}; T = 20 °C, pH = 4.8; Øs = 200 µm.

According to the kinetic study, the amounts of Cr(III) and Pb(II) adsorbed by BFS increased progressively with stirring speed until reaching 150 rpm, then decreased (Fig. 2). The weakening of the adsorption process is surely caused by the strong agitation, which slowed down the external diffusion of the metal ions. Based on these findings, we estimate that 150 rpm is the optimal stirring speed for Cr(III) and Pb(II) ion adsorption.

Effect of pH

The pH of the medium is an important factor in this process since it impacts both the shape of the ions and the surface of the adsorbent [21]. In this context, we have worked at different pH levels, namely 3.2, 4.2, 4.8, and 5.4. The experimental conditions applied are: C_O = 30 mg l^{-1}; T = 20 °C, V_{ag} = 150 rpm; Øs = 200 µm.

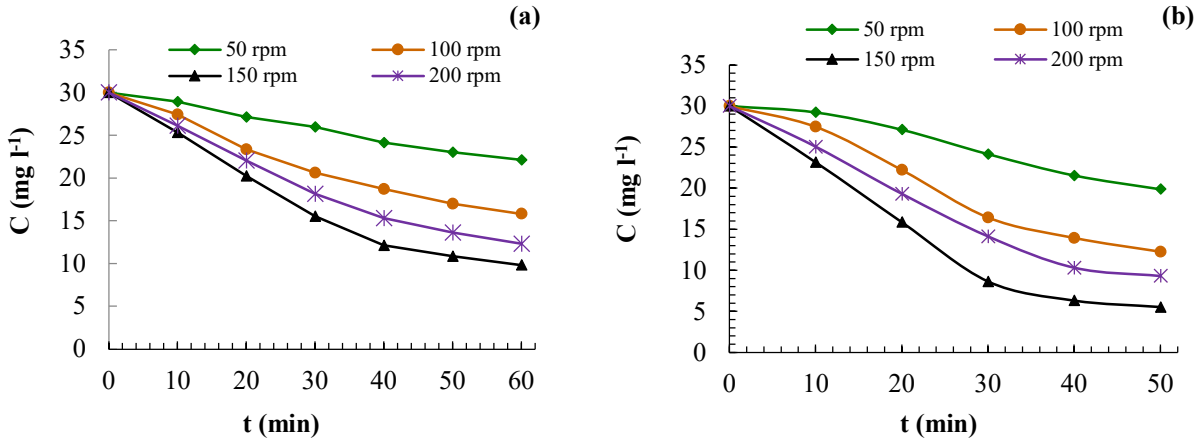

Fig. 2. Effect of agitation speed: (b) Cr(III) adsorption, (b) Pb(III) adsorption.

According to the experimental data, the adsorption of Pb(II) and Cr(III) ions is unfavorable for solutions with a pH of 3.2 (Figs. 3a and 3b). This evolution is caused by the presence of H^+ protons, which hinder the adequate transfer of metal ions from the solution to the adsorbent; in addition, the charge of the adsorbent is positive (pH < pHzpc) [33].

From Figs. 3a and 3b, it has been noticed that the adsorption is more efficient from pH 4.2 to 5.4, and it is better at pH 4.8. This result is due to the negative charge of the surface of the adsorbent (pH > pHzpc), which favored the adsorption under the effect of attractive interaction. Based on these results, we consider 4.8 to be the perfect pH for the adsorption of Cr(III) and Pb(II) ions.

Effect of Contact Time

The contact time effect on examined the metal ions adsorption was performed over a time ranging from 0 to 180 min under specific experimental conditions, namely pH 4.8, V_{ag}: 150 rpm, T: 20 °C, $Ø_s$: 200 µm, M_S: 1 g and C_0: 30 mg l^{-1} (Fig. 4a).

The kinetic study showed that the adsorption of the studied metal ions is initially considered important, but then it decreases with time until the total stop of the process at 50, 60, and 80 min, respectively, for Pb(II), Cr(III), and the Cr-Pb mixture (Fig. 4a). The adsorption process progression is certainly generated by the presence of vacant adsorption sites and by the presence of negative charges on the surface of the adsorbent (the effect of electrostatic attraction) [21,33]. The total stop of the adsorption process reveals that the free

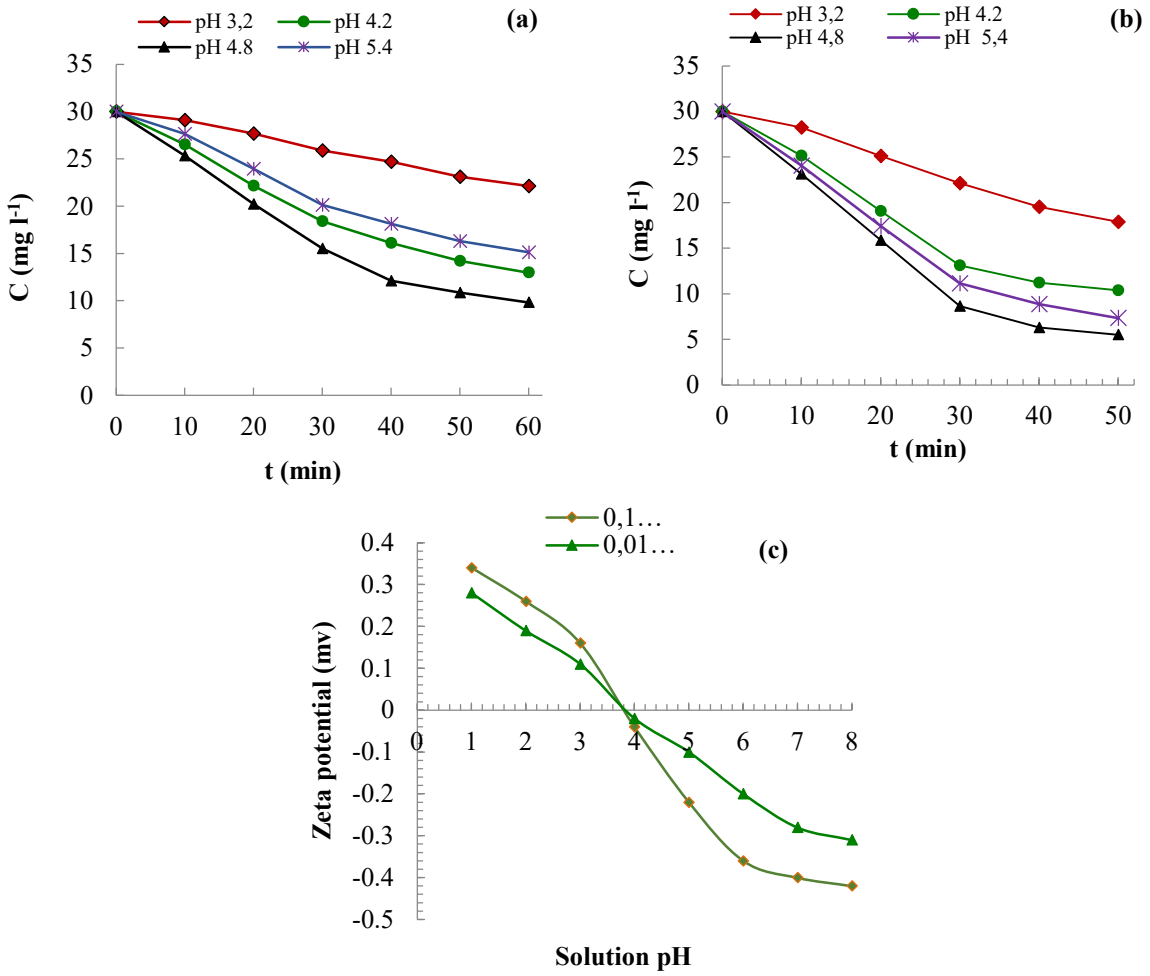

Fig. 3. Effect of pH: (a) Cr(III) adsorption, (b) Pb(III) adsorption, (c) Zeta potential as a function of solution pH.

adsorption sites are saturated. This outcome led us to consider, respectively, 50, 60, and 80 min, the equilibrium times for the adsorption of Cr(III), Pb(II), and the Cr-Pb binary mixture on the BFS. It should be noted that the delay in the thermodynamic equilibrium observed during the adsorption of the binary mixture is caused by the competition between the Cr(III) and Pb(II) ions at the solid-liquid interface [34].

Effect of Adsorbent Dosage

The adsorbent dosage influence on these adsorption processes was accomplished under the following experimental conditions: pH: 4.8, V_{ag}: 150 rpm, T: 20 °C, $Ø_s$: 200 µm, C_0: 30 mg l^{-1}, and M_S from 0.2 to 1.4 g.

From Fig. 4b, it has been shown that the metal ion adsorption rate increases with the mass of the adsorbent. This phenomenon can be explained by the increase in active adsorption sites [35]. It was also indicated that at high adsorbent masses (m > 1 g), the adsorption rate was slightly reduced. This regression was probably caused by the agglomeration of solid particles [36]. Accordingly, 1 g opted as the optimal mass of adsorbent for this process.

Effect on Initial Concentration

The effect of the initial concentration on the adsorption of trivalent chromium, lead and the binary mixture Cr-Pb on BFS was accomplished in particular operating conditions, namely pH 4.8, V_{ag}: 150 rpm, T: 20 °C, $Ø_s$: 200 µm, M_S 1 g, and C_0 ranges from 10 to 120 mg l^{-1}.

The experimental adsorption isotherms and the adsorption rates are represented in Fig. 5. The plot produced by the function qe = f(C_0) revealed that the isotherms passed through a minimum at low concentrations, then increased as the initial concentration increased until the adsorbent was saturated. The adsorbed quantities values of Cr(III), Pb(II), Cr(III) in the mix, Pb(II) in the mix, and the Pb-Cr mixture, respectively, corresponding to 43.16, 50.12, 17.05, 22.66, and 39.91 mg g^{-1}.

The isotherms first passed through a minimum at low concentrations, then increased as the initial concentration increased until the adsorbent was saturated, as shown in Fig. 5a. The maximum adsorbed amounts of Pb(II) and Cr(III) in the mixture are lower than in mono-adsorption (Fig. 5a). This phenomenon is probably caused by the competition between metal ions for vacant sites [34]. In the mixture, the amount of Pb(II) adsorbed is greater than the amount of Cr(III). Because the atomic and ionic radii of Pb(II) are lower than those of Cr(III), it adsorbs more effectively [37].

From Fig. 5b, it was revealed that the most important elimination rate is at low concentrations. This performance is prompted by the availability of vacant adsorption sites at low concentrations, which systematically contributed to the increase in the adsorption rate [34]. On the other hand, in the presence of many metal ions, the active sites gradually saturate and become inaccessible. Consequently, the rate of elimination automatically regresses [21].

Finally, the adsorption capacity of BFS is comparable to or greater than the capacity of other adsorbents used in solution Pb(II) and Cr(III) removal processes (Table 2).

Adsorption Isotherms

Adsorption isotherms were investigated in order to understand the adsorption behavior of Cr(III), Pb(IL), and the Cr-Pb mixture on slag (BFS). In this context, we applied the experimental data models widely used in adsorption processes, namely Freundlich [36], Langmuir [28], and Temkin [33]. The linear form of their equation is represented by Eqs. (5) to (7), successively.

$$\log q_e = \log k + \frac{1}{n}\log C_e \quad (5)$$

$$\frac{C_e}{q_e} = \frac{1}{q_{max}} C_e + \frac{1}{q_{max} b} \quad (6)$$

$$qe = B_T ln A_T + B_T ln Ce \quad (7)$$

$$B_T = \frac{RT}{b_T} \quad (8)$$

Where q_e: amount adsorbed at equilibrium (mg g^{-1}), C_e: solution concentration at equilibrium (mg l^{-1}), q_{max}: maximum capacity adsorbed (mg g^{-1}), K_F: Freundlich isotherm constant, 1/n: empirical parameter Freundlich associated with the intensity of the adsorption process and b is the thermodynamic constant of the adsorption equilibrium (l mg^{-1}), A_T is Temkin isotherm equilibrium binding constant (l g^{-1}), b_T is Temkin isotherm constant kJ mol^{-1}), R universal gas constant, T is Temperature at 298 K and B_T is Constant

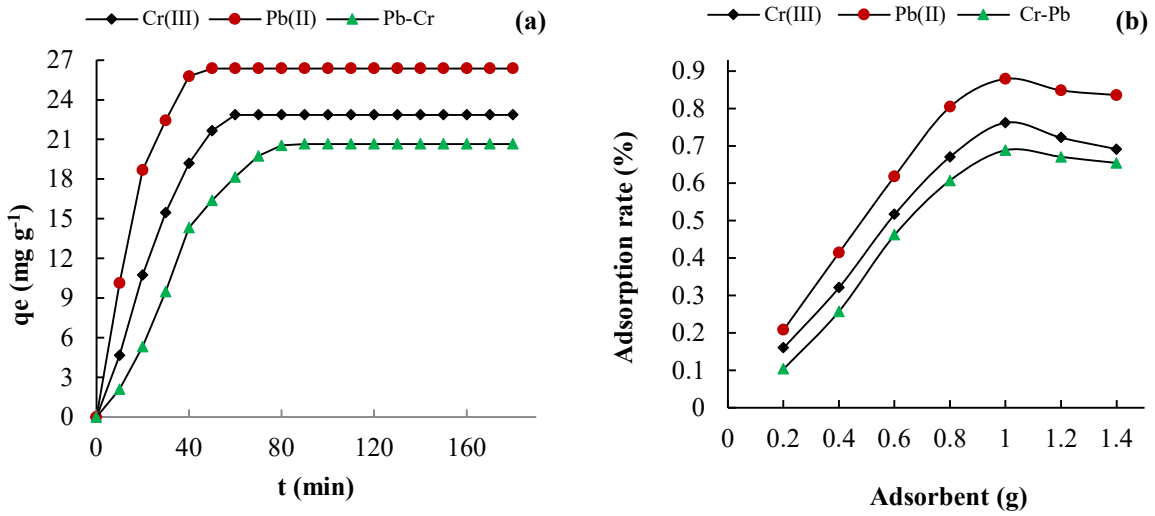

Fig. 4. (a) Effect of contact time, (b) effect of adsorbent mass.

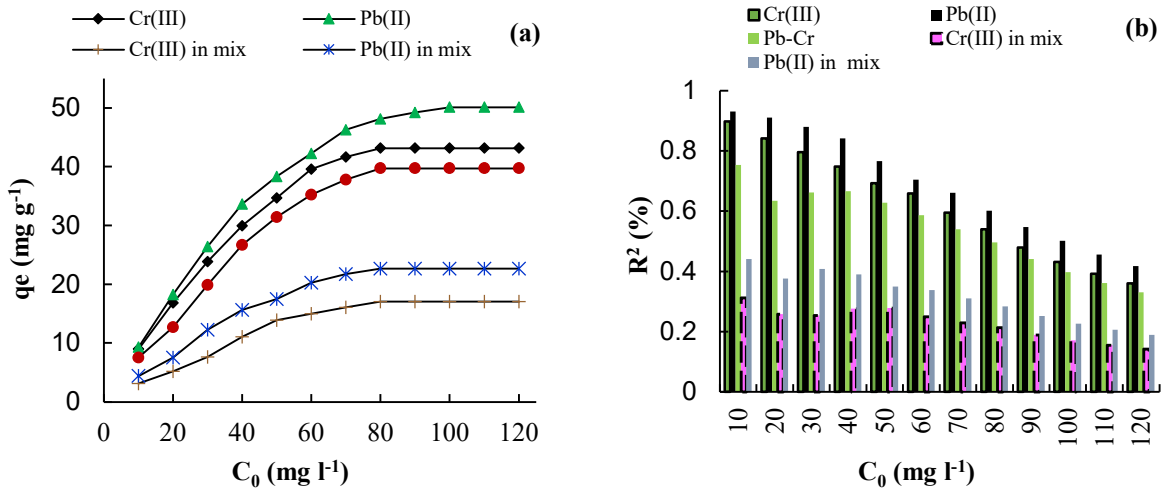

Fig. 5. Effect of initial concentration: (a) adsorption kinetics (b) Elimination rate.

Table 2. The Adsorption Capacity of Various Adsorbents for Pb(II) and Cr (III) Ions

Adsorbent	Metal ion	q_{max} (mg g^{-1})	Ref.
Cellulose acetate/polycaprolactone	Pb(II)	70.5	[38]
Oxidized coconut fiber biochar	Pb(II)	326	[39]
Tobacco leaves	Pb(II)	24.7	[40]
Activated carbon from Cocos Nucifera waste	Pb(II)	48.26	[41]
Pineapple peel fiber	Pb(II)	70.29	[42]
Jatropha curcas	Cr(III)	22.88	[43]
Water hyacinth biochar	Cr(III)	7	[44]
Amine-based polymer	Cr(III)	8	[45]
Nanofibrils	Cr(III)	69.84	[46]

related to the heat of sorption.

The parameter values of the Freundlich, Langmuir, and Temkin adsorption models are listed in Table 3. Their plots (Figs. 6, 7, 8) are presented in the electronic supplementary material.

In accordance with the results obtained (Table 2), it was

Table 3. Isotherm Parameters Adsorption by BF Slag

Models	Parameters	Cr(III)	Pb(II)	Pb-Cr_{mix}	$Cr(III)_{mix}$	$Pb(II)_{mix}$
Freundlich	K_F (mg g^{-1}) (ml mg^{-1})^1	10.61	14.64	4.88	1.86	2.92
	n	2.54	2.9	1.84	1.76	1.87
	R^2	0.93	0.90	0.92	0.91	0.91
Langmuir	q_{max} (mg g^{-1})	43.47	50.50	41.66	18.86	22.72
	b (l mg^{-1})	0.21	0.78	0.03	0.15	0.07
	R^2	0.99	0.99	0.99	0.99	0.99
	R_L	0.41-0.07	0.22-0.03	0.7-0.2	0.4-0.06	0.58-0.13
Temkin	A_T (l g^{-1})	2.06	3.62	1.67	1.35	1.31
	B_T (kJ mol^{-1})	10.94	11.62	11.32	10.64	10.71
	R^2	0.92	0.93	0.92	0.91	0.91

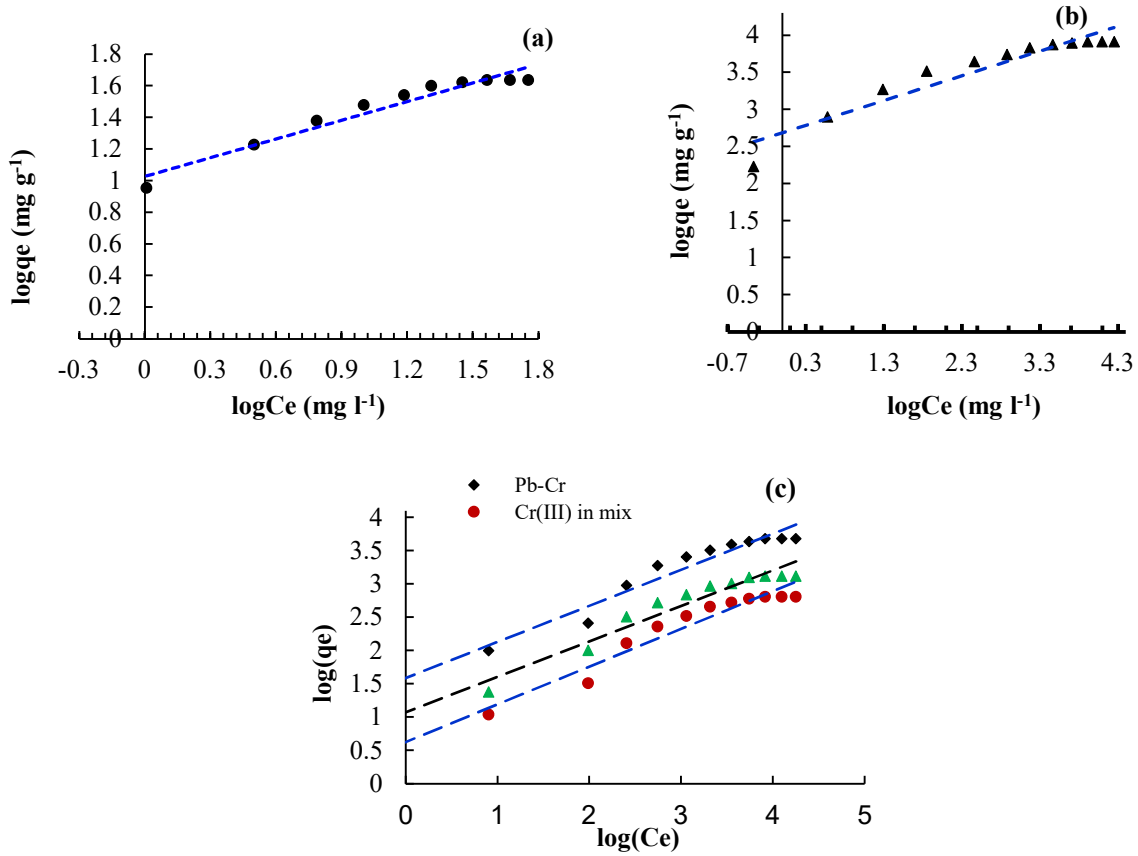

Fig. 6. Presentation of Freundlich model: (a) trivalent chromium, (b) lead, (c) chromium-lead mixture.

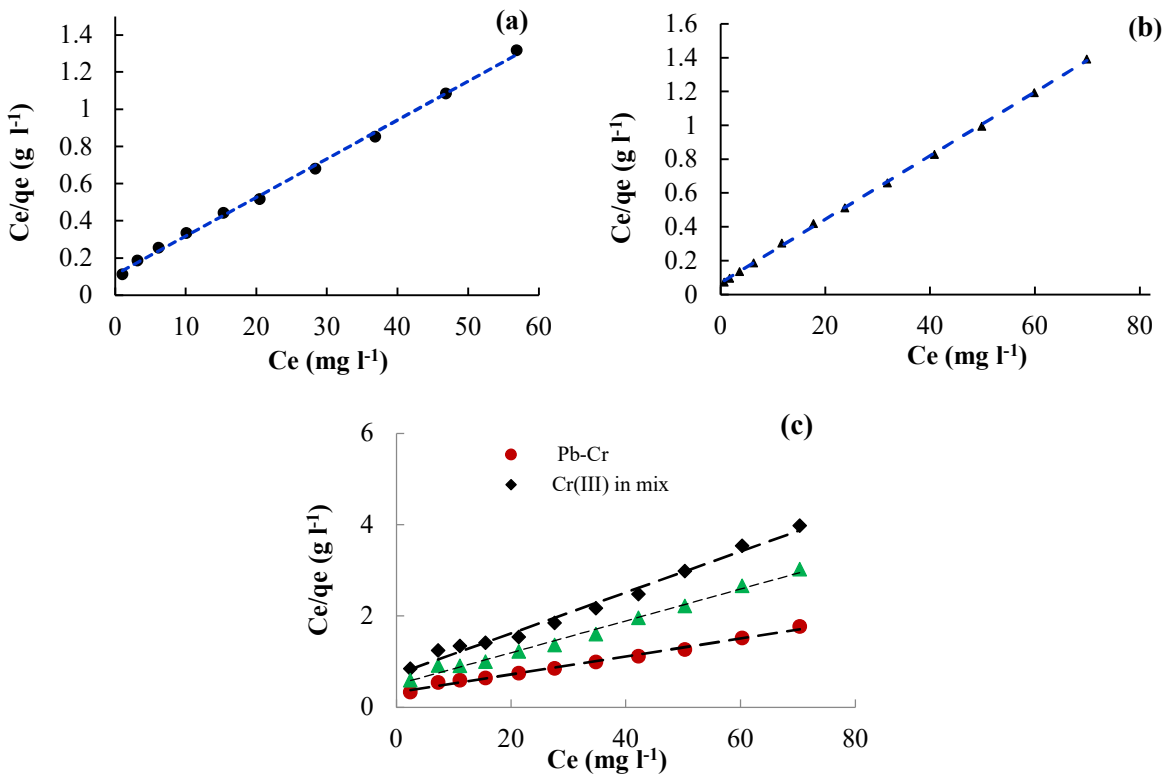

Fig. 7. Presentation of Langmuir model: (a) trivalent chromium alone, (b) lead alone, (c) chromium-lead mixture.

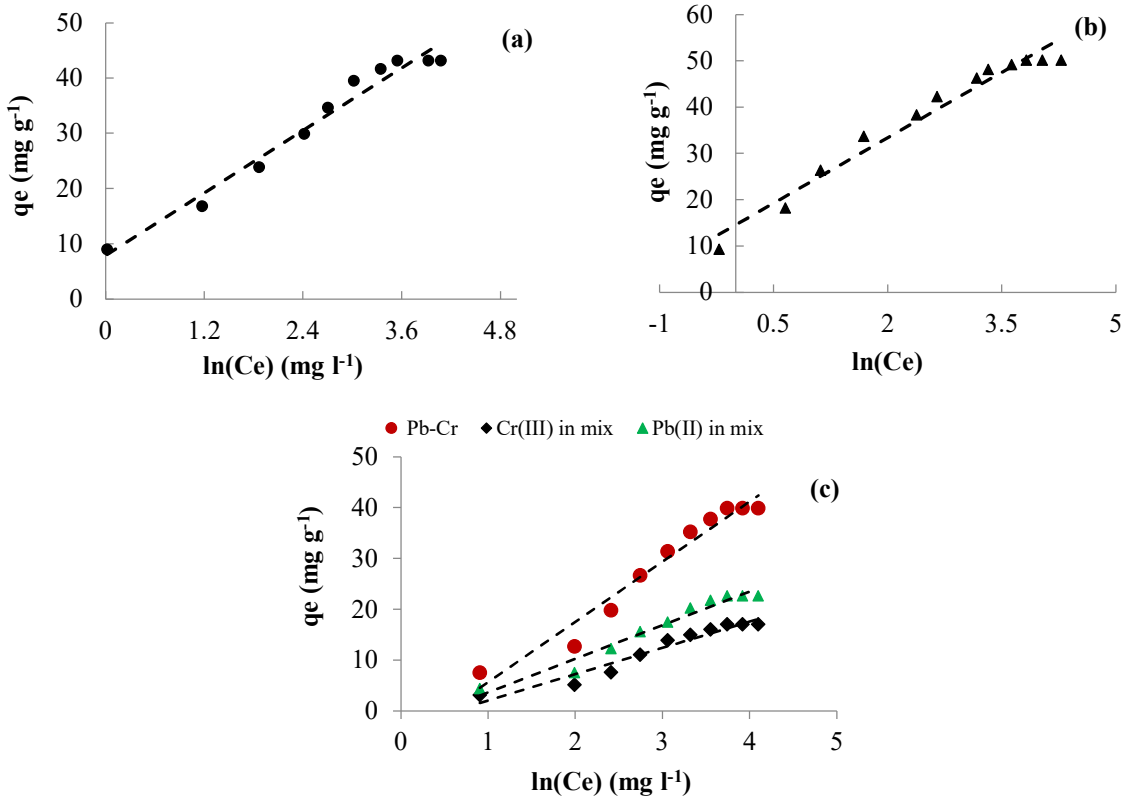

Fig. 8. Presentation of Temkin model: (a) trivalent chromium alone, (b) lead alone, (c) chromium-lead mixture.

observed that the Langmuir model is the most suitable for the adsorption process of all the metal ions analyzed. Indeed, the correlation coefficients of the Langmuir model are higher than the correlation coefficients of the Freundlich and Temkin models. In addition, the theoretical adsorbed quantities of the pollutants considered are very close to the experimental capacities [47].

From Figs. 9a, 9b, and 9c, it was noticed that the graphs of the adsorption isotherms of the Langmuir model described a classic L-type isotherm. The adsorption takes place gradually until reaching a saturation level. This result confirmed that Cr(III) and Pb(II) adsorption, either alone or in a binary mixture, occurred on a homogeneous monolayer surface [21]. The Freundlich model parameter value (n) shows that the process is favorable [33]. The value of the Temkin model parameter (Bt) indicates that adsorption is favorable [21] and the interaction between adsorbate and adsorbate is physical [33].

From the literature, it has been shown that the nickel removal on the blast furnace slag in solution is also achieved on a monolayer homogeneous surface [21]. Similarly, Mn(II) adsorption on steel slag in an aqueous solution [48] and Cu(II) adsorption on basic oxygen furnace slag [49].

According to the literature [21,29,33], the R_L separation factor can also inform us about the quality of the solid exploited. Indeed, it has been explained that the adsorption nature depends on the value of the one-dimensional parameter R_L. That is to say, it is favorable if $0 < R_L < 1$, unfavorable if $R_L > 1$, linear if $R_L = 1$ and irreversible if $R_L = 0$.

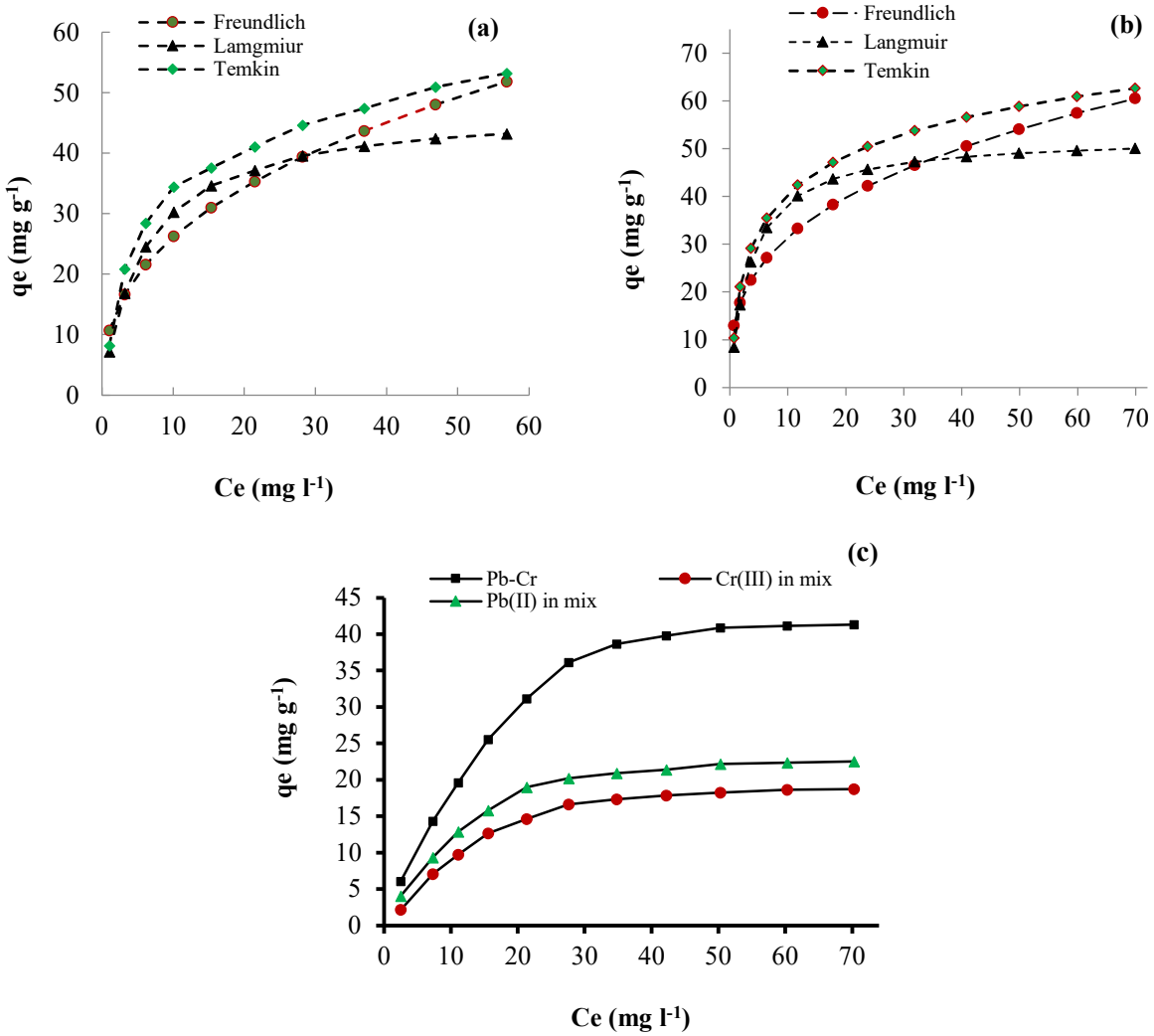

Fig. 9. Presentation of the Langmuir Isotherms: (a) Cr(III) in the mix, (b) Pb(II) in mix, (c) Cr-Pb.

The separation factor R_L is obtained from the following equation (Eq. (7)).

$$R_L = \frac{1}{1+C_0 b} \quad (7)$$

Where b is the Langmuir isotherm constant (l mg^{-1}) and C_0 is the initial concentration (mg l^{-1}).

From Table 2, it was observed that the separation factor values R_L for all the elements examined are between 0 and 1. This outcome confirms that the adsorption processes carried out in solution on the slag are favorable [50].

Adsorption Kinetics

Two mathematical models, namely pseudo-first order and pseudo-second order [16], were used to analyze the adsorption kinetics of Cr(III), Pb(II), and the Pb-Cr mixture on BFS. It is important to note that these two models are designed to demonstrate the control mechanisms of the reaction on the surface of the adsorbent [51]. Equations (8) and (9) represent the pseudo-first and pseudo-second-order models, respectively.

$$\log(q_e - q) = -k_L t + log q_e \quad (8)$$

$$\frac{t}{q} = \frac{1}{k_b q_e^2} + \frac{t}{q_e} \quad (9)$$

Where q_e is the adsorbed quantity at equilibrium (mg g^{-1}), q is the amount of metal ions adsorbed at time t (mg g^{-1}), t is the time of adsorption process, k_L is the constant pseudo-first-order kinetic equation (min^{-1}) and k_b is the constant of pseudo-second order speed equation (min^{-1}).

The plots of these models are reproduced in Figs. 10 and 11. Their kinetic parameters are reported in Table 4.

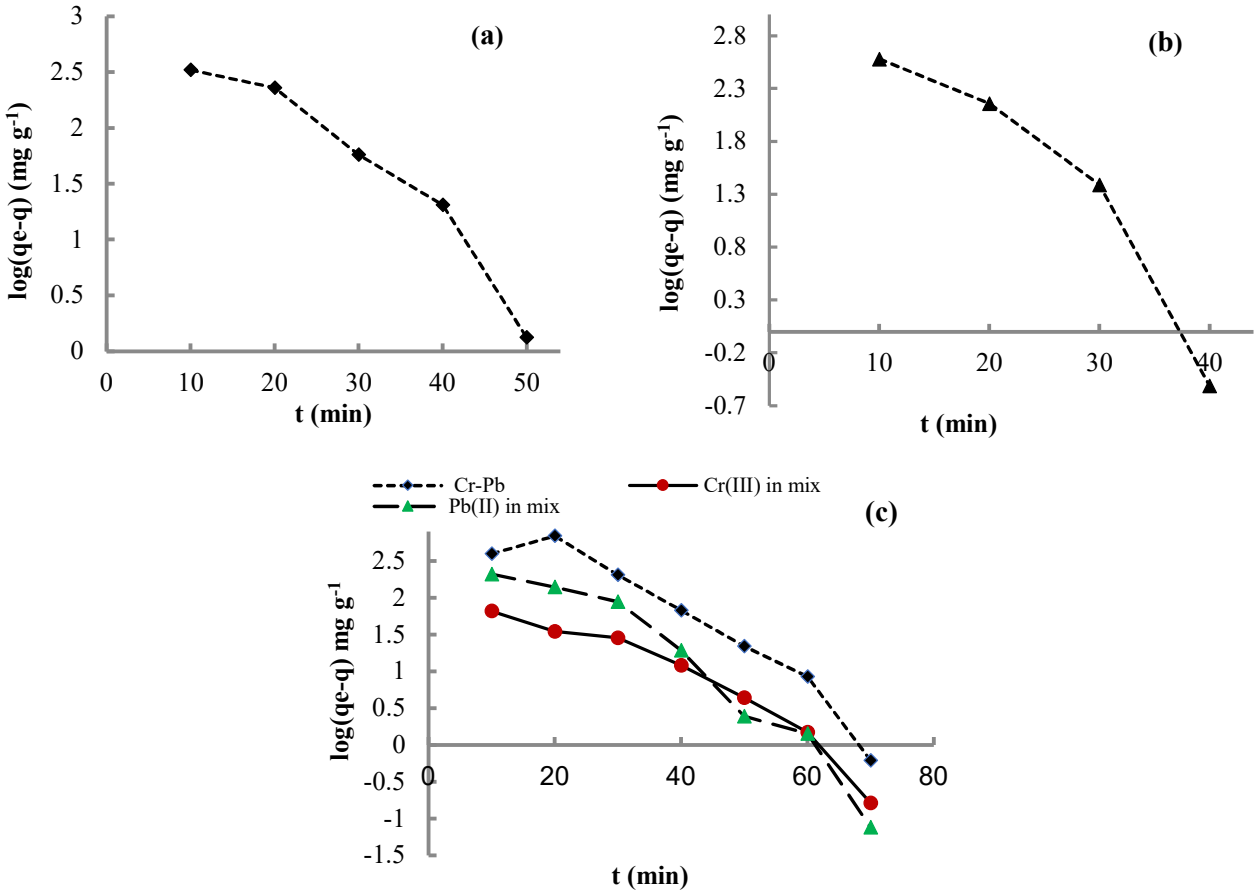

Fig. 10. Pseudo first-order kinetics: (a) Cr(III) alone, (b) Pb(II) alone, (c) Cr-Pb mixture.

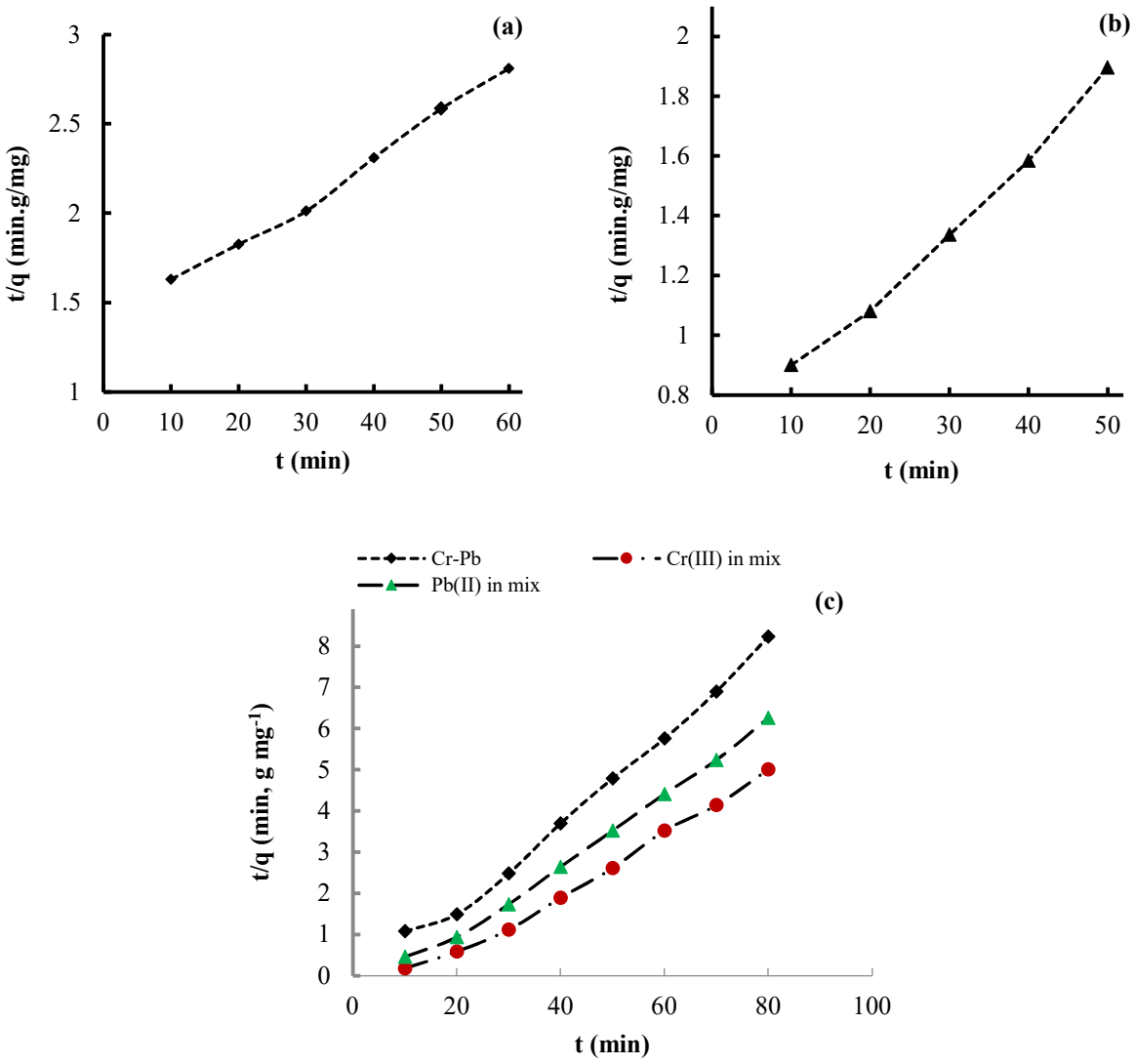

Fig. 11. Pseudo second order kinetics: (a) Cr(III) alone, (b) Pb(II) alone, (c) Cr-Pb mixture.

Table 4. Pseudo First and Second Order Parameters

Pollutant	Pseudo first order			Pseudo second order		
	K_1 (min^{-1})	qe_{theo} (mg g^{-1})	R^2	K_b (g mg^{-1} min^{-1})	qe_{theo} (mg g^{-1})	R^2
Pb-Cr	0.082	42.93	0.90	4.3×10^{-24}	40.19	0.99
$Cr(III)_{mix}$	0.047	19.12	0.91	4.8×10^{-2}	17.15	0.99
$Pb(II)_{mix}$	0.056	23.84	0.93	6.8×10^{-2}	22.71	0.99
Cr(III)	0.067	47.89	0.89	5.48×10^{-4}	44.45	0.99
Pb(II)	0.095	56.84	0.88	7.9×10^{-4}	50.68	0.99

From the collected data, it was shown that the pseudo-second-order model presents a better adjustment of the experimental points ($R^2 = 0.99$) than the pseudo-first-order model ($R^2 \leq 0.90$). It was also revealed that the theoretical maximum quantity adsorbed from the pseudo-second-order model is closer to the experimental value (Table 4). The k_b constants affirm that the adsorption on the BFS is better in the case of lead. The perfect correlation of the pseudo-second-order model revealed that the effects of electrostatic interactions play a preponderant role in the adsorption processes [52]. These results mean that the elimination of Pb(II), Cr(III), and the Cr-Pb mixture in solution follows pseudo-second-order kinetics.

From the bibliography, the removal of Cu(II) and Pb(II) ions from flotation wastewater by steel slag has been reported to follow pseudo-second-order kinetics [26]. Similarly, for the removal of cobalt(II) ions in aqueous solutions by oxalated blast-furnace slag [23].

Diffusion Study

The mechanism of Pb(II), Cr(III), and Cr-Pb mixture transfer from solution to BFS was determined by studying the limiting stages of adsorption kinetics, namely external diffusion [33] and intraparticle diffusion [34]. These limiting steps were examined through Eqs. (10) and (11), respectively.

$$logC_t = k_{ext}t + C_{Ext} \quad (10)$$

$$q = k_{Int}\sqrt{t} + C_{int} \quad (11)$$

where C_t is the residual concentration at time t (mg l^{-1}), q is the quantity adsorbed at the time t (min), k_{ext} is the film diffusion coefficient (min^{-1}); k_{int} is the diffusion rate constant in the pores (mg m^{-1} $min^{-½}$) and C_{Int} and C_{Ext} are the intercepts with the Y axis relative to internal and external diffusion.

The graphs representing the external and internal diffusion are reproduced, respectively, in Figs. 12 and 13. Their parameters are given in Table 5.

According to Weber and Morris [44], it was stated that internal diffusion completely controls the adsorption process if the line is linear and passes through the origin [53].

According to Figs. 12b, 13b, and Table 5, it has been indicated that the plots resulting from the function $q = f(t^{1/2})$ are multilinear and do not pass through the origin with correlation coefficients greater than 0.9.

From this result, we can conclude that intraparticle diffusion is not the only mechanism controlling the adsorption processes. Indeed, the adsorption processes performed are also influenced by external diffusion, given that the correlation coefficients obtained from the function $log(C_t) = f(t)$ are greater than 0.9 (Table 5) [54]. From this result, we understand that the adsorption processes are controlled by external diffusion followed by intraparticle diffusion.

Temperature Effect

The influence of the medium's temperature on the adsorption process is very important [29]. Indeed, it contributes to the fixation of the pollutant on the adsorbent surface and informs us about the nature and feasibility of the

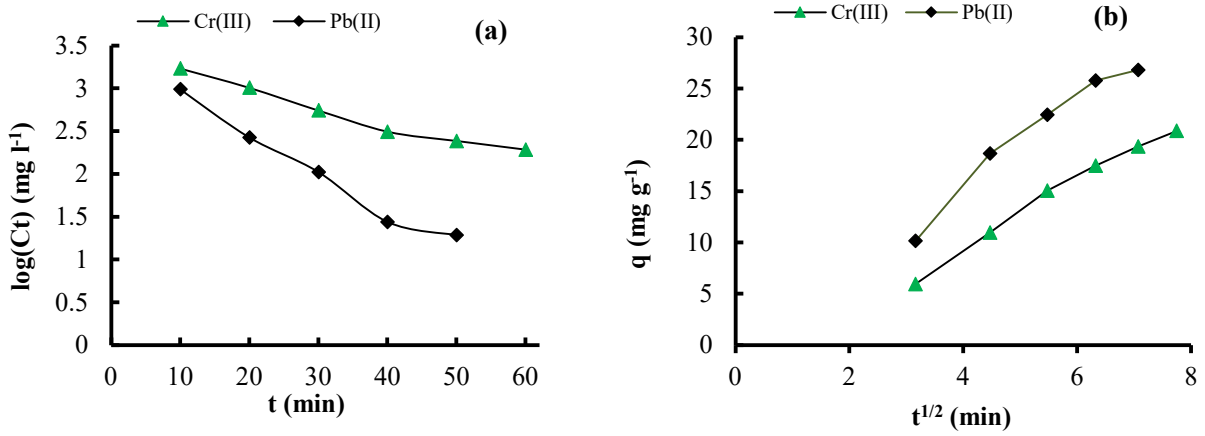

Fig. 12. Diffusion study of Pb and Cr alone: (a) External Diffusion, (b) intraparticle diffusion.

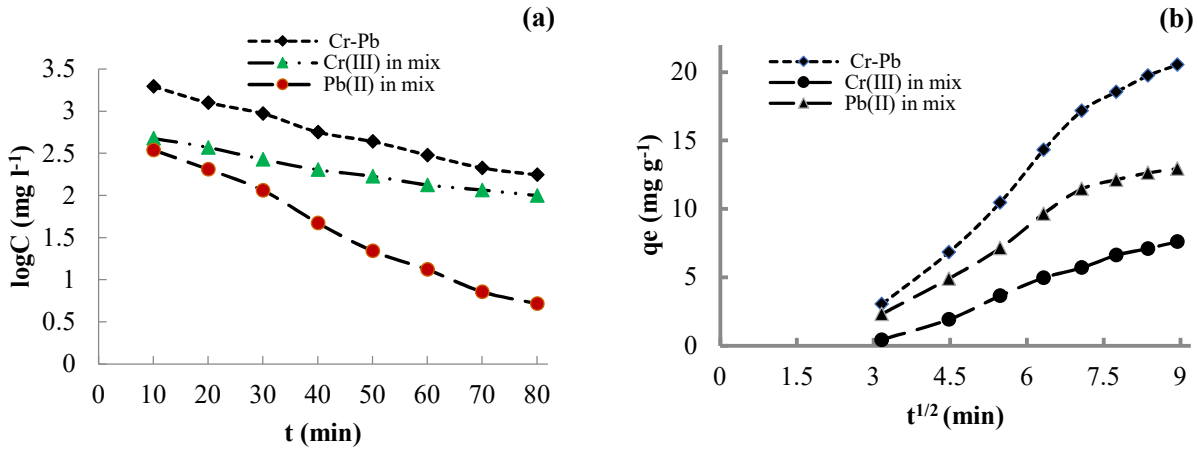

Fig. 13. Diffusion study of the Pb-Cr mixture: (a) External Diffusion, (b) intraparticle.

Table 5. Values of diffusion parameters

Polluant	Intraparticle diffusion			External diffusion		
	C_{Int}	K_{Int} (mg g^{-1} min^{-1})	R^2	C_{Ext}	K_{Ext} (min^{-1})	R^2
Pb-Cr	6.87	3.24	0.98	3.41	0.015	0.99
$Cr(III)_{mix}$	3.51	1.28	0.99	2.76	0.009	0.99
$Pb(II)_{mix}$	3.7	1.99	0.69	2.81	0.027	0.99
Cr(III)	3.79	3.29	0.98	3.35	0.043	0.97
Pb(II)	1.94	4.28	0.95	3.37	0.019	0.96

process. The effect of temperature on the adsorption of Cr(III), Pb(II), and the Cr-Pb mixture was studied at 20, 30, 40, and 50 °C (Fig. 11).

From Fig. 11a, it was indicated that the adsorption capacities of the metal ions studied are maximum at 20 °C and begin to decrease as the temperature increases. This effect leads to the prediction that the adsorption process is exothermic [55]. The weakening of interactions between metal ions and active adsorption sites could explain the regression of adsorption processes with increasing temperature. Additionally, the exothermic nature of the process reduces the efficiency of adsorption at higher temperatures.

To better understand the effect of temperature on the adsorption processes carried out, it was essential to determine the values of the thermodynamic parameters, such as ΔG, ΔS, and ΔH. These parameters were defined by the following equations [21]:

$$\Delta G^0 = -RTlnk_d \quad (12)$$

$$\Delta G^0 = \Delta H^0 - T\Delta S^0 \quad (13)$$

$$lnk_d = \frac{\Delta H^0}{R} \times \frac{1}{T} + \frac{\Delta S^0}{R} \quad (14)$$

where ΔG is Gibbs energy, ΔH is the enthalpy variation, ΔS is entropy variation, T is the absolute temperature (K), R is the universal gas constant; K_d is the distribution coefficient (l g^{-1}).

The plot of the function $\ln k_d = f(1/T)$ is represented by Fig. 11b. The values of the thermodynamic parameters are presented in Table 6.

From Table 5, it has been indicated that the values of the calculated thermodynamic parameters of all the examined adsorption processes are negative. The negative values of ΔG° at different temperatures inform us about the spontaneity and feasibility of the accomplished adsorption processes [19,21]. The negative values of ΔH° reveal that the elimination of the metal ions studied is exothermic [19]. The negative values of ΔS° show the decrease in randomness at the solid/liquid interphase of the studied adsorption processes [33].

The absolute values of the enthalpy change (ΔH° < 40 kJ mol^{-1}) imply that the physical interaction mechanism plays a determining role in the process of the metal ions' adsorption on the BFS [56]. This outcome is also justified by the calculated values of free enthalpies (-20 < ΔG° < 0 kJ mol^{-1}) [57]. It is essential to mention that with the rise in temperature, the movement of metal ions multiplies, which causes the return of metal ions from the adsorbent to the adsorbate [58], which leads to the regression of the adsorption capacity at high temperatures.

Desorption Study

The desorption of the pollutants from the charged solid adsorbents is a considerable step [28,46]. Indeed, it allows us to reuse the adsorbent and avoid regenerating another type of pollution.

With this in mind, we proceeded to the desorption of the binary mixture (Cr-Pb) adsorbed on the slag of the blast furnace operated. The desorption rate was calculated from Eq. (15).

$$desorption\ rate = \frac{q_{des}}{q_{ads}} \times 100 \quad (15)$$

Where q_{ads} is the adsorbed quantity at equilibrium (mg g^{-1}) for the cycle I and q_{ads} is the desorbed quantity at equilibrium (mg g^{-1}) of each cycle.

Figure 12 shows the effect of eluents and distilled water on the desorption of the binary mixture (Cr-Pb). Table 6 displays the performance of the adsorption/desorption processes of the binary mixture on the blast furnace slag (BFS).

The experimental data revealed that the process of desorption of binary mixtures (Cr-Pb) from the surface of the saturated slag is more efficient with HCl at 0.1 N. Desorption yields are calculated to be 96.26% (HCl), 80.45% (H_2SO_4), 46.49 (HNO_3), and 29.23% (H_2O) (Fig. 12a).

The adsorption/desorption tests carried out on the saturated BFS indicated that the first 4 cycles are more Following this outcome, hydrochloric acid (HCL: 0.1 N) was selected as the regeneration eluent.

Table 6. Thermodynamic Parameters and Activation Energy

Polluant	T (K)	ΔG° (kJ mol^{-1})	ΔH° (kJ mol^{-1})	ΔS° (J $mol^{-1}.K^{-1}$)
Cr(III)	293	-17.26	-6.98	-29.14
	303	-17.69		
	313	-18.06		
	323	-18.49		
Pb(II)	293	-15.49	-5.52	-18.62
	303	-15.92		
	313	-16.32		
	323	-16.68		
Cr-Pb	293	-11.21	-5.16	-18.08
	303	-11.40		
	313	-11.68		
	323	-11.97		

efficient. The adsorption/desorption rate for all cycles examined decreased from 93.12 to 56.72% (Table 7S). The reduction in the rate of desorption is certainly caused by the loss of mass of the adsorbent [33] and or the degradation of the surface of the adsorbent (reduction of the adsorbent power).

The good desorption of Cr(III) and Pb(II) ions is due to the physical nature of the adsorption process, where the adsorbate species are partially held to the adsorbent with relatively weak bonds.

CONCLUSIONS

This work argues that treated blast furnace slag (BFS) is a considerable adsorbent for the removal of metal ions in an aqueous medium. Its characterization indicates that it consists of silica, lime, and alumina with a considerable specific surface (325.6 $m^2 g^{-1}$). The pH value corresponding to PZC is about 3.8. The tests carried out reveal that the efficiency of the process of adsorption of the metal ions studied depends largely on the contact time, speed of agitation, pH of the solution, the temperature of the solution, the particle size of the adsorbent, initial concentration, and mass of the adsorbent. The maximum sorption of Pb(II) alone, Cr(III) alone, and Cr-Pb in a mixture on the BFS was observed after 50, 60, and 80 min, respectively, at pH 4.8, agitation speed of 150 rpm, the temperature of 20°C, the solid particle size of 200, and mass of adsorbent 1 g. Furthermore, the adsorption rate of Pb(II) in the mixture is greater than that of Cr(III). The experimental data indicated that the adsorption isotherms of Pb(II), Cr(III), and Pb-Cr in the binary mixture are quite consistent with the Langmuir model (R^2: 0.99). The values of the Freundlich (n) and Langmuir (R_L) parameters certify that the adsorption processes studied are favorable. The Temkin model parameter (Bt) indicates that the adsorption processes carried out are physical. The kinetic study of adsorption revealed that the elimination of the metal ions considered follows the pseudo-second-order model and that their transfers from the solution to the adsorbent are controlled by external and intraparticle diffusion. The interpretation of theoretical and experimental data indicates that electrostatic interaction is the determining mechanism in these processes. The influence of temperature showed that the adsorption processes carried out are favorable, spontaneous, exothermic, and less entropic. BFS can be used adequately for four cycles in the treatment of wastewater containing Cr(III) and Pb(II) ions.

The proposed adsorption process is simple, inexpensive, efficient, and respectful of the environment, which could contribute positively to keeping the water safe from harmful metals. In addition, the blast furnace slags used in several treatments could be reused as backfill materials and road construction materials.

REFERENCES

[1] J.A.S. Costa, R.A. de Jesus, D.O. Santos, J.F. Mano, L.P.C. Rom˜ao, C.M. Paranhos. Microporous Mesoporous Mater. 291 (2020) 109698.
[2] M. Hossain, P.K. Patra, Ecol. Indic. 117(2020) 106668.
[3] M. Karamipour, S. Fathi, M. Safari, Int. J. Environ. Anal. Chem. 10 (2021) 1915299.
[4] J. El-Gaayda, F.E. Titchou, R. Oukhrib, P.-S. Yap, T. Liu, M. Hamdani, R. A. Akbour, J. Environ. Chem. Eng. 9 (2021) 106060.
[5] W.S. Chai, J.Y. Cheun, P.S. Kumar, M. Mubashir, Z. Majeed, F. Banat, S.-H. Ho, P.L. Show, J. Clean. Prod. 296 (2021) 126589.
[6] M.E. Mahmoud, E.A. Saad, M.A. Soliman, M.S. Abdelwahab, J. 145 (2019) 1102.
[7] Y.C. López, G.A. Ortega, E. Reguera, Chem. Eng. J. Adv. 11 (2022) 100297.
[8] S. Bolisetty, M. Peydayesh, R. Mezzenga, Chem. Soc. Rev. 48 (2019) 463.
[9] M.A. Barakat, Arabian J. Chem. 4 (2011) 361.
[10] M. Li, K. Hu, J., Wang, J. Eng. Appl. Sci. 68 (2021) 35.
[11] S.M. Safwat, M.E. Matta, J. Eng. Appl. Sci. 68 (2021) 48.
[12] M. Karamipour, S. Fathi, M. Safari, Int. J. Environ. Anal. Chem. 191 (2021) 5299.
[13] E. Sharifpour, H.Z. Khafri, M. Ghaedi, A. Asfaram, R. Jannesar, Ultrason. Sonochem. 40 (2018) 373.
[14] M. Abaszadeh, R. Hosseinzadeh, M. Tajbakhsh, S. Ghasemi, J. Mol. Struct. 1261 (2022) 132832.

[15] X. Guan, X. Yuan, Y. Zhao, J. Bai, Y. Li, Y. Cao, Y. Chen, T. Xiong, J. Colloid Interface Sci. 612 (2022) 572.
[16] N. Belachew, H. Hinsene, Appl. Water Sci. 10 (2020) 10.
[17] M. Dolatabadia, M. Mehrabpour, M. Esfandyari, H. Alidadi, M. Davoudi, Chemom. Intell. Lab. Syst. 181 (2018) 72.
[18] C. Liu, H.-X. Zhang, J. Environ. Chem. Eng. 10 (2022) 107393.
[19] M. Hazrati, M. Safari, Environ. Prog. Sustainable Energy 39 (2020) e13411.
[20] A.K. Thakur, R. Singh, R.T. Pullela, V. Pundir, Mater. Today: Proc. 57 (2022) 1468.
[21] T. Chouchane, O. Khireddine, A. Boukari, J. Eng. Appl. Sci. 68 (2021) 00039.
[22] S.H. Kim, S. Jeong, H. Chung, K. Nam, Chemosphere 263 (2021) 128337.
[23] Q.T. Ngoc Le, E.L. Vivas, K. Cho, J. Ind. Eng. Chem. 95 (2021) 57.
[24] C. Li, X. Li, Y. Yu, Q. Zhang, L. Li, H. Zhong, S. Wang, J. Ind. Eng. Chem. 105 (2022) 63.
[25] S.H. Kim, H. Chung, S. Jeong, K. Nam, J. Clean. Prod. 279 (2021) 123451.
[26] L. Wang, P. Fu, Y. Ma, X. Zhang, Y. Zhang, X. Yang, Miner. Eng. 183 (2022) 107593.
[27] Y. Xue, H. Houa, S. Zhu, J. Hazard. Mater. 162 (2009) 391.
[28] W. Yuan, J. Kuang, M. Yu, Z. Huang, Z. Zou, L. Zhu, J. Hazard. Mater. 405 (2021) 124261.
[29] T. Chouchane, S. Chouchane, A. Boukari, A. Mesalhi, J. Mater. Environ. Sci. 6 (2015) 924.
[30] E. Yilmaz, R.M. Alosmanov, M. Soylak, RSC Adv. 5 (2015) 33801.
[31] M. Khan, E. Yilmaz, M. Soylak, J. Mol. Liq. 224 (2016) 639.
[32] S. Brunauer, P.H. Emmett, E. Teller, J. Am. Chem. Soc. 60 (1938) 309.
[33] T. Chouchane, A. Boukari, Anal. Bioanal. Chem. Res. 9 (2022) 381.
[34] F. Cherono, N. Mburu, B. Kakoi, Heliyon 7 (2021) e08254.
[35] E. Sabanovic, M. Memic, J. Sulejmanovic, A. Selovic, Pol. J. Chem. Technol. 22 (2020) 46.
[36] A. Malakahmad, S. Tan, S. Yavari, J. Chem. 2016 (2016) 1.
[37] A.H. Sulaymon, S.E. Ebrahim, M.J. Mohammed-Ridha, Environ. Sci. Pollut. Res. 20 (2012) 175.
[38] R.R. Aquino, M.S. Tolentino, R.M.P.D. Elacion, R. Ladrillono, T.R.C. Laurenciana, B.A. Basilia, IOP Conf. Ser. Earth Environ. Sci. 191 (2018) 012139.
[39] Q. Wu, Y. Xian, Z. He, Q. Zhang, J. Wu, G. Yang, X. Zhang, H. Qi, J. Ma, Y. Xiao, L. Long, Sci. Rep. 9 (2019) s41598-019-52554-2.
[40] V. Yogeshwaran, A.K. Priya, Materials Today: Proceedings 37(2021) 489.
[41] P. Baskaran, M. Abraham, Sustain. Energy Technol. Assess. 53 (2022) 102709.
[42] X. Hu, M. Zhao, G. Song, H. Huang, Environ. Technol. 32 (2011) 739.
[43] A.C. Gonçalves Jr., H. Nacke, D. Schwantes, M.A. Campagnolo, A.J. Miola, C.R.T. Tarley, D.C. Dragunski, F.A.C. Suquila, Environ. Sci. Pollut. Res. 24 (2017) 21778.
[44] Md. Abul Hashem, M. Hasan, Md. Abdul Momen, S. Payel, Md. S. Nur-A-Tomal, Environ. Sustainability Indic 5 (2020) 100022.
[45] P. Albino Kumar, M. Ray, S. Chakraborty, Chem. Eng. J. 149 (2009) 340.
[46] S. Huang, C. Ma, Y. Liao, C. Min, P. Du, Y. Zhu, Y. Jiang, React. Funct. Polym. 106 (2016) 76.
[47] C. Fan, B. Du, Y. Zhang, S. Ding, Y. Gao, M. Chang, J. Geochem. Explor. 176 (2017) 50.
[48] S. Mohebali, D. Bastani, H. Shayesteh, J. Mol. Struct. 1176 (2019) 181e193.
[49] M.S.M. Zahar, F.M. Kusin, S.N. Muhammad, Procedia Environ. Sci. 30 (2015) 145.
[50] Y. Xue, S. Wu, M. Zhou, Chem. Eng. J. 231 (2013) 355.
[51] H. Bensalah, S.A. Younssi, M. Ouammou, A. Gurlo, M.F. Bekheet, J. Environ. Chem. Eng. 8 (2020) 103807.
[52] Y. Deng, S. Huang, C. Dong, Z. Meng, X. Wang, Bioresour. Technol. 303 (2020) 122853.S.
[53] F. Raji, M. Pakizeh, Appl. Surf. Sci. 301 (2014) 568.
[54] A.K. Sakhiya, V.K. Vijay, P. Kaushal, Bioresour.

Technol. Rep. 17 (2022) 100920.

[55] R. Foroutan, F.S. Khoo, B. Ramavandi, S. Abbasi, Desalination Water Treat. 82 (2017) 146.

[56] T. Liu, Y. Lawluvy, Y. Shi, J.O. Ighalo, Y. He, Y. Zhang, P.-S. Yap, J. Environ. Chem. Eng. 10 (2022) 106502.

[57] M. Antunes, V.I. Esteves, R. Guégan, J.S. Crespo, A.N. Fernandes, M. Giovanela, Chem. Eng. J. 192 (2012) 114.

[58] H. Liu, F. Zhang, Z. Peng, Sci. Rep. 9 (2019) 3663.